https://doi.org/10.5194/nhess-2024-170
Preprint. Discussion started: 5 March 2025

Natural Hazards and Earth System Sciences
Discussions

Characteristics and disaster implications of offshore active faults around Nan'ao Island, the northern South China Sea

Hu Yi[1, 2], Wenhuan Zhan[1, 2, *], Xiaodong Yang[1], Jian Li[1], Xiaochuan Wu[3, 4], Jie Sun[1], Yantao Yao[1], Jiaxian Huang[1, 2], Zelong Ju[1, 2]

[1]Key Laboratory of Ocean and Marginal Sea Geology, South China Sea Institute of Oceanology, Chinese Academy of Sciences, Guangzhou 510301, China

[2]University of Chinese Academy of Sciences, Beijing 100049, China

[3]National Joint Local Engineering Research Center for Shale Gas Exploration and Development, Chongqing Institute of Geology and Mineral Resources, Chongqing 401120, China

[4]Key Laboratory of Shale Gas Exploration, Ministry of Natural Resources, Chongqing Institute of Geology and Mineral Resources, Chongqing 401120, China

Correspondence to: Wenhuan Zhan (whzhan@scsio.ac.cn)

Abstract. Frequent earthquakes in China's Nan'ao Sea, the fault structure and its activity pattern in this region have been the focus of attention. Using high-resolution seismic reflection data, this study uncovers a large graben offshore Nan'ao island. The northwest boundary of the graben is a seaward-dipping normal fault, which spreads upward in the form of fault-propagating folds and forms a gentle submarine slope. The southeast boundary of the graben is a landward-dipping normal fault, manifesting as a growth fault that cuts to the seabed. Analysis of activity shows the fault/fold activity rates on both sides of the graben are similar, suggesting they are part of a unified active tectonic system. Simulations of fault propagation folds on the northwest side of the graben reveal that within the sedimentary strata that have been investigated, there should exist three phases of normal dip sliding (approximately 20 meters per phase), a prolonged period of quiescence ensues between the sliding phases, this result supports the periodic and intermittent character of the fault activity and indicates the presence of seismic-scale strain. Based on these insights, the research explores the activity mode of fault association in the Nan'ao sea area, it proposes a seismogenic model that emphasizes the controlling and driving role of gravity in shallow deformation characteristics.

1. Introduction

In the coastal areas of southeastern China, numerous destructive seismic events of magnitude 6 or

https://doi.org/10.5194/nhess-2024-170
Preprint. Discussion started: 5 March 2025


Natural Hazards and Earth System Sciences
Discussions
Open Access
EGU

higher have occurred in history. In particular, two strong earthquakes, both of magnitude 7 or higher, occurred in the sea off Nan'ao Island: one M7.0 in 1600 and another M7.3 in 1918 (Fig. 1). The 1918 Nan'ao M7.3 earthquake triggered the only recorded seismic tsunami event in China during the 20th century. The seismic activity in southeastern coastal region is widely believed to be intricately linked to the dynamic behavior of the Littoral Fault Zone(LFZ), a significant offshore deep fault zone. Therefore, an in-depth investigation into the active faults within the coastal seas of this region will help to understand the causes of seismicity in the southeast coastal region of China, and also provide a scientific foundation for disaster prevention and mitigation efforts in the region.

The seismogenic location of the fault is usually several kilometers to tens of kilometers below the surface. The complexity of the deep rock environment and the extreme physical conditions make it extremely difficult to detect the fault activity rule directly with instruments. In addition, the coverage of sea water further increases the difficulty of the field investigation of fault in sea areas. Therefore, studies on the LFZ of the Nan'ao offshore mainly adopt geophysical methods for exploration. For example, Zhao et al. (2004) and Xia et al. (2020) used tomography techniques to reveal the deep crustal structure around Nan'ao Island. However, while these large-scale studies provide valuable insights, they do not offer the detailed information required for accurate earthquake hazard assessment. Zhang et al. (2024) studied the shallow performance of the coastal fault zone near Nan'ao in detail by using the ship-borne air gun source multi-channel seismic profile, revealing the relationship between fault geometry and fault activity properties. However, they did not deeply explore the direct relationship between the shallow submarine characteristics and seismic activity, leaving room for further research.

Fault seismicity is a complex process, involving phenomena such as fault geometry, kinematic properties and activity periodicity. These phenomena manifest not only on the surface but also closely linked to deep crustal activities. For example, fault geometry can influence the mode of earthquake rupture (Zhang et al., 2022; Zhang et al., 2023; Wang et al., 2024), kinematic properties are related to seismic energy release (Melgar et al., 2023; Zhao and Yao, 2018), cyclical activity may indicate earthquake recurrence patterns (Julve et al., 2024; Melgar et al., 2023; Grützner et al., 2017). Currently, the discussion and analysis of the correlation between shallow fault characteristics and deep processes in the LFZ, located off the coast of Nan'ao Island, are still a critical link that needs to be supplemented in earthquake disaster assessment.

In a recent investigation of the activity of the LFZ in the Taiwan Strait region, researchers observed a

https://doi.org/10.5194/nhess-2024-170
Preprint. Discussion started: 5 March 2025


Natural Hazards and Earth System Sciences
Discussions

near-seabed monoclinal fold deformation at the location of the main fault in the Quanzhou sea section (Fig. 1). These deformations have been attributed to reactivation of the normal basement fault and present typical characteristics of normal fault-propagation fold (Yi et al., 2022) (Fig. 3b). A widely used kinematic model of fault-propagation fold, the trishear model (Erslev, 1991; Allmendinger, 1998; Hardy and Ford, 1997; Zehnder and Allmendinger, 2000), by analyzing the morphology of shallow folds, allows for the assessment of seismic activity that may occur on blind faults (Allmendinger and Shaw, 2000; Pratt et al., 2002; Shaw et al., 1999; Suppe, 2002). Based on the above research revelations, we believe it is feasible to infer information about deep activities by the shallow surface fine analysis of the LFZ in the Taiwan Strait area. Establishing appropriate deep-shallow correlation is the key to using superficial features to gain insight into deep activity information.

Recent small earthquakes have clustered in the study area (Fig. 1 and Fig. 2), intensive seismic activity can not only reveals deep structural traces but also corresponds to the basement faults and surface deformation above it. In this paper, we apply a mini-multichannel seismic data acquisition technique of a marine sparker source with submeter resolution, with the goal of obtaining high-resolution seismic profiles of shallow sedimentary layers at the same survey line location as the air gun source multichannel seismic survey used by Xia et al. (2020). Through fine analysis of the structure of the shallow sedimentary layer, combined with deep tectonic studies, we aim to reveal the regularity of fault/fold activity in the study area, and clarify the structural geometry and kinematic evolution of the area. The results of the study will provide a new perspective for understanding the relationship between recent tectonic activity patterns in the study area and earthquakes and consequent tsunamis.

https://doi.org/10.5194/nhess-2024-170
Preprint. Discussion started: 5 March 2025

Natural Hazards and Earth System Sciences
Discussions

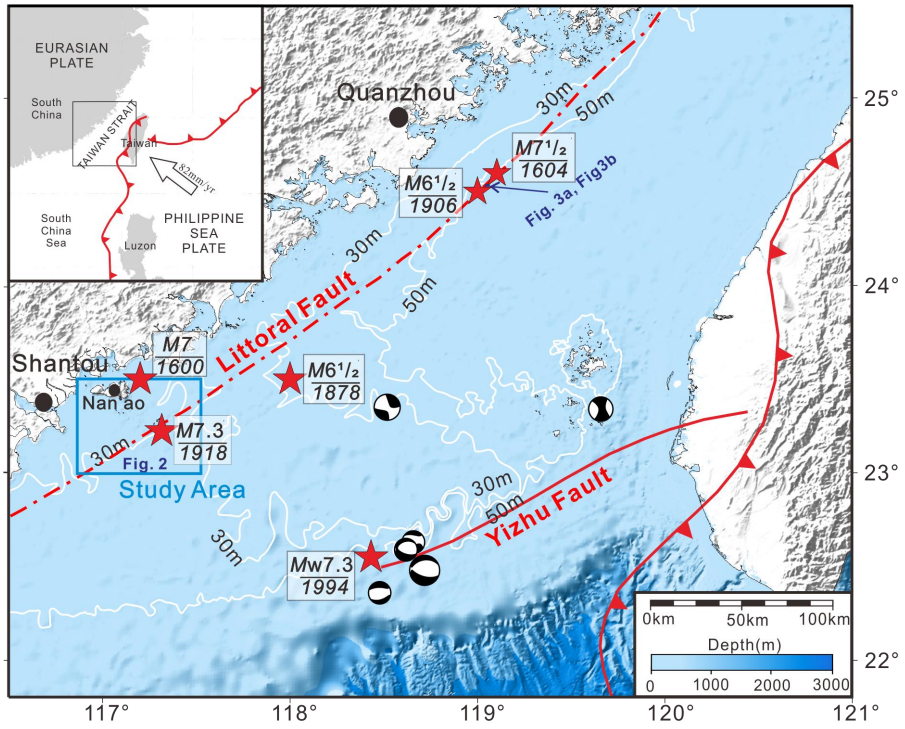

Figure 1. Geotectonic map of the sea area off Nan'ao and adjacent areas. Red pentagrams indicate recent historical earthquakes, locations according to Zhang et al. (2020), and Xu et al. (2006); location of the Littoral Fault according to Liu (1985), location of the Yizhu Fault according toWang et al. (2011); seismic mechanism solution courtesy of global CMT (www.globalcmt.org).

2. Tectonic geological background

The coastal regions of Fujian and eastern Guangdong are located on the southeastern edge of the Eurasian Plate, influenced by the combined effects of the Indian Ocean Plate and Philippine Sea Plate. Throughout a lengthy tectonic evolutionary process, these areas have been driven by multiple tectonic mechanisms (Morley, 2016; Xu et al., 2022; Li et al., 2019), with temporal overlaps (Qiu et al., 2021). Since the early Mesozoic, the coastal region has been in a long-term extrusion process owing to the intra-terrestrial collisional orogeny, with deep mantle uplift at the land margin, crustal uplift and erosion, and widespread exposure of late Yanshanian granites in the coastal areas of Fujian In the late Mesozoic, under the subduction of the Paleo-Pacific Plate and its eastward rollback, significant lithospheric extension and thinning occurred in the eastern part of the South China Block, accompanied by medium-acidic and medium-basic magmatism, leading to the formation of a major magmatic belt

https://doi.org/10.5194/nhess-2024-170
Preprint. Discussion started: 5 March 2025


Natural Hazards and Earth System Sciences
Discussions

over 1000 km long with a NE-NNE strike in southeastern China (Xu et al., 2022; Li and Li, 2007; Li et al., 2023). The development of bimodal volcanic-intrusive complexes, alkaline granites, and basic dykes along the southeast coast of China indicates a Late Cretaceous extensional environment (Li, 2000; Charvet et al., 1994; Wang et al., 2017). With further crustal rifting, NE-NNE trending faults became active, leading to the formation of a series of half-graben-style marginal rifts, which are the embryonic forms of the Taixi Basin. However, some believe that such Mesozoic-Cenozoic half-graben basins were formed under specific compressive tectonic condition (Li et al., 1988). Since the Neogene, the Philippine Sea Plate has been colliding and subducting beneath the southeastern side of the Eurasian Plate, placing the Fujian-Taiwan area under a NWW-oriented principal stress field. In the late Miocene, 6.5 Ma ago, arc-continent collision orogeny occurred on Taiwan Island, and the area west of the Central Mountain Range entered the stage of foreland basin evolution (Chou and Yu, 2002; Lin et al., 2003). During the Miocene-Early Pleistocene, possibly extending to Late Pleistocene, along the southeastern coastal area of Zhangpu, Fujian, basaltic eruptions occurred along the coastal NE-trending supracrustal fault, forming a series of small, sporadically distributed NE-trending eruptive landforms. Since the Holocene, there have been several records of transgression and retrogression along the coast of South China, with coastal uplift as the general trend, and intermittent crustal uplift was implied by the multilevel marine terraces in the coastal area (Pedoja et al., 2008; Pedoja et al., 2011). The correlation between the distribution of magma, active faults and natural earthquakes in the study area is obvious (Xia et al., 2020).

The current definition of the LFZ is a "belt" concept with a width of tens of kilometres. This structural zone extends in a NE-NEE direction along the coast of the South China, and two phases of the normal fault are developed, the older phase of the normal fault is strongly active in the rift basin rifting period, and it has a large throw, averaging 0.5 km and ranging up to nearly 2 km (Cao et al., 2018; Chou and Yu, 2002); the newer phase of normal faults has smaller throw, less than 100 m (Chou and Yu, 2002). It has been indicated that the centers of extension within the Taiwan Strait are inconsistent (Zhang et al., 2018; Lin et al., 2003). The location of the faults studied in this paper is highly coincident with the location of the Littoral Fault (LF) delineated by Liu (1985; Fig. 1), which is roughly distributed along the bathymetric contour lines of 30–50 m depth, which represent a submarine linear step, indicative of the latest activity of the LF. In addition, the LF is defined as the demarcation line between the Zhejiang-Fujian uplift zone and the Taiwan Strait land-margin rift zone, which belongs to the edge of

https://doi.org/10.5194/nhess-2024-170
Preprint. Discussion started: 5 March 2025

the two major tectonic units. Among them, the Taixi Basin is a half graben basin, with the LF as its western boundary, which is significantly smaller in scale compared to the fault on the eastern boundary. Additionally, a series of discrete northwest-oriented faults intersect the northeast-oriented structures (Zhang et al., 2018), and the interaction zone of these faults is the active zone of historical large earthquakes (Xia et al., 2020).

3. Data and methods

The Nan'ao Offshore research area is centered around Nanpeng Islands, with water depths ranging between 10 m and 60 m. The locations of (LF) in the study area (Figs. 1 and 2) are approximately marked based on satellite imagery and gravity and magnetic anomalies (Liu, 1985). The South China Sea Institute of Oceanology (SCSIO), Chinese Academy of Sciences (CAS), acquired deep-penetrating seismic reflection profiles reaching the basement of the region using airgun seismic sources in July 2016. These profiles consist of 11 NW–SE lines crossing the LF and 3 SW–NE parallel lines (Xia et al., 2020) (Fig. 2). In May 2019, SCSIO of CAS conducted another data collection in the same research area using high-resolution multichannel seismic reflection data with small channel spacing generated by sparker source. This dataset serves as the primary data for this study and includes four NW–SE profiles labeled as N6, N7, N8, and N9 (Fig. 2), totaling 108km. The Geo-Spark 2000X sparker source system and digital acquisition system produced by the Dutch company Geo Marine Survey Systems were utilized. The data acquisition system included Geo-Sense Multi Channel Streamers, equipped with 2 Multi-Trace 24 acquisition modules and the Multi-Trace Server acquisition software. The cable was a nearly 150 m long fully digital towed cable (deployed at the stern during data acquisition). The integrated navigation positioning system comprised the Hypack 2013 navigation software system and the Trimble SP351 DGPS receiver, ensuring a positioning accuracy of <5m. The seismic source triggering was controlled by Hypack, and the on-site acquisition system parameters are detailed in Table 1. This system stored seismic data in the standard Society of Exploration Geophysicists Y (SEG-Y) format. Within the profile depth range of 0–450 ms, the sparker seismic source data obtained had a main frequency of 332 Hz and a minimum vertical resolution of 1.2 m.

https://doi.org/10.5194/nhess-2024-170
Preprint. Discussion started: 5 March 2025

Natural Hazards and Earth System Sciences
Discussions

Table 1. The main parameters of the seismic acquisition system.

Seismic source	Minimum offset /m	Number of coverage	Sample interval /ms	Receptor interval /m	Shot interval /m	Source Sinking depth /m	Cable Sinking depth /m
sparker 2 000 J	0	12	0.2	3.125	6.25	0.4	0.3

The data were processed using the seismic data processing software RadExpro, together with a self-programmed software system, to obtain high signal-to-noise ratio seismic profile data. The process and methods of data processing mainly include defining the observation system, static correction, noise eliminiation, amplitude compensation, deconvolution, velocity analysis, multiple wave attenuation, pre-stack time migration, post-stack processing, filter and gain.

With the gradual increase in the density and coverage of seismic station deployment, by 2018, the quality and positioning accuracy of natural earthquake monitoring in the southeastern coastal region of China have been significantly improved. This study utilized earthquake catalog data from the study area between 2018 and 2023 to analyze the relationship between the Littoral Fault Zone (LFZ) and seismogenic structures (Fig. 2). The historical earthquake locations and magnitudes shown in Fig. 1 are derived from Ref.

This paper explains seven stratigraphic units, T1–T7, aiming to illustrate and quantify the geometric morphology of faults and folds. Through precise measurement of vertical distances on seismic profiles, we present them as individual vertical throw distribution plots (T-Z plot) for quantitative analysis of fault activity(Muraoka and Kamata, 1983; Jackson et al., 2016; La Bruna et al., 2018). As the fault propagates upward, the pre-existing ductile layer (such as sedimentary layer) respond in the form of monoclines to the activity of deep basement faults (Erslev, 1991; Withjack et al., 1990; Coleman et al., 2019), the triangular shear model (Fig. 3d) can be used to explain the geometric features and kinematic processes of fault-propagation folds(Hardy and Mcclay, 1999; Jin and Groshong, 2006; Erslev, 1991). this model uses P/S ratio to illustrate the relative rates of fault propagation and uses the apex angle of the triangular shear zone to control the width of fault propagation folds(Jin and Groshong, 2006; Hardy and Ford, 1997; Erslev, 1991; Allmendinger, 1998). In this model, the defined amplitude of monoclines corresponds directly to the vertical throw of basement fault activity (Fig. 3d). We similarly measure the amplitude of monoclines in detail and present them as separate fold amplitude distribution maps (A-Z diagram) to quantify the activity of faults and related folds. Additionally, we quantify the amplitude of

https://doi.org/10.5194/nhess-2024-170
Preprint. Discussion started: 5 March 2025

Natural Hazards and Earth System Sciences
Discussions
Open Access
EGU

compression folds in the triangular shearing zone to illustrate the degree of compression deformation, also displayed as fold amplitude distribution maps (A-Z diagram). Furthermore, we employ the balanced cross-section method to restore the position and morphology of sedimentary strata before undergoing compression deformation, thus facilitating a better understanding of the kinematic processes of adjacent strata near faults. It is worth noting that, according to the results of engineering drilling in this area, the sedimentary layers above the basement are unconsolidated layers, with little variation in seismic velocity. The time-depth was converted for the corresponding profile. The average acoustic velocity was 1800m/s for the sedimentary layer and 1500m/s for the water column.

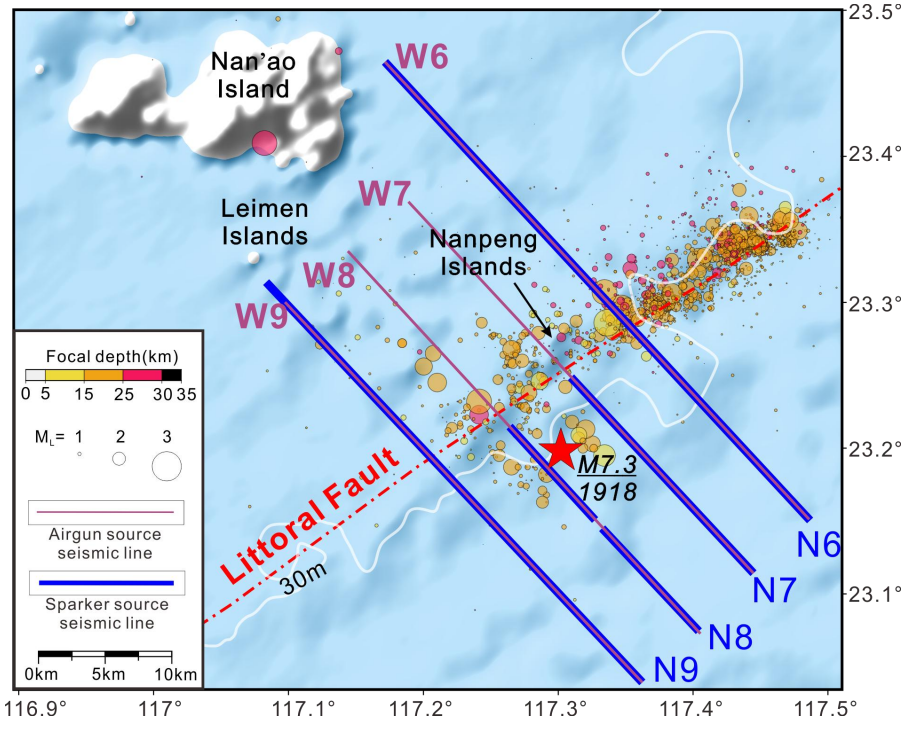

Figure 2. Location map of survey lines in the study area. N6–N9 are the sparker seismic source reflection seismic lines of this acquisition, W6–W9 are the G-gun source reflection seismic lines acquired by Xia et al. (2020). The red pentagram are the locations of the 1918 M7.3 Earthquake as located by Xu et al. (2006). The small circles denote the seismic events of 2018–2023, which are obtained from the Fujian Earthquake Agency.

https://doi.org/10.5194/nhess-2024-170
Preprint. Discussion started: 5 March 2025

Natural Hazards and Earth System Sciences
Discussions

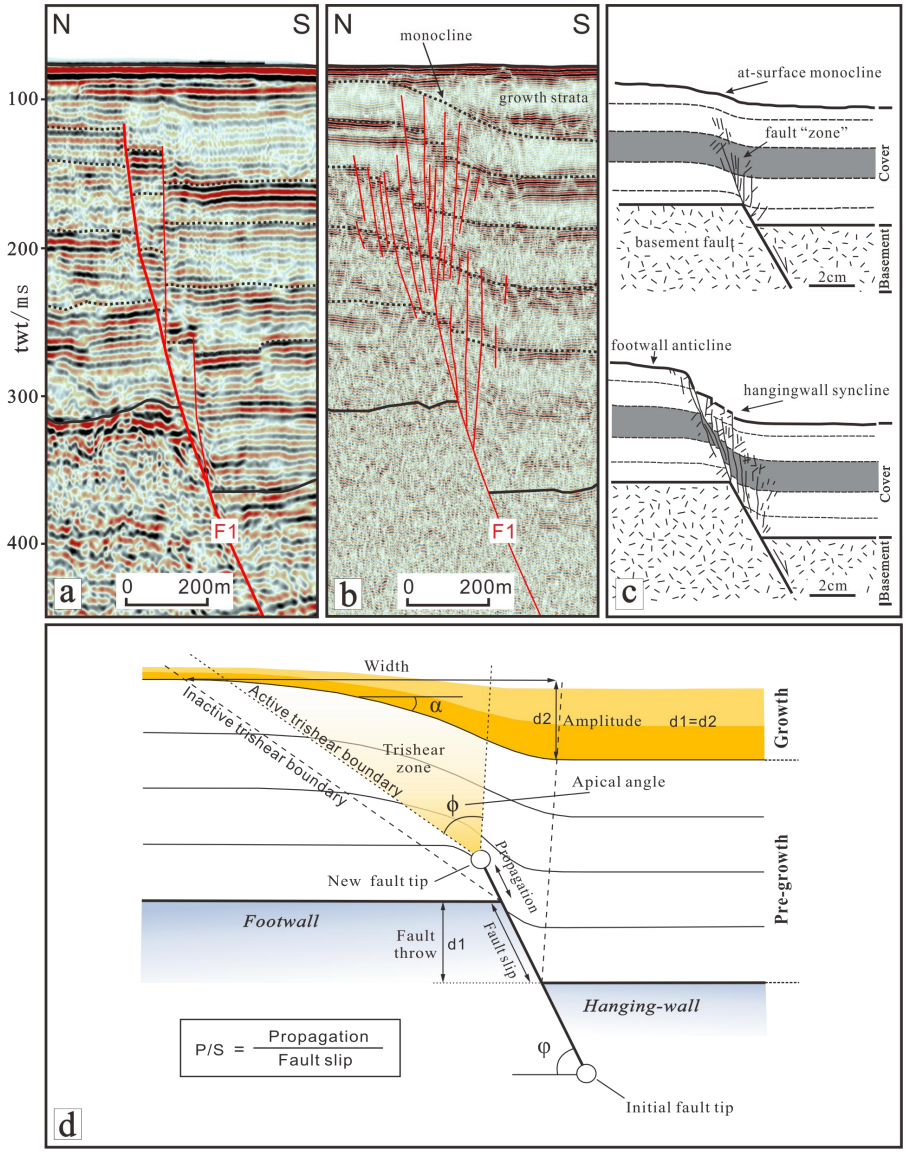

Figure 3. (a) GI-gun source mini-mutichannel seismic reflection profile imaging of LF in Quanzhou offshore section (Yi et al., 2022); (b) Sparker source mini-mutichannel seismic reflection profile imaging of LF in Quanzhou offshore section (Yi et al., 2022); (c) Clay deformation above the concealed basement faults, modified from Withjack et al. (1990); (d) Schematic diagram of the basic elements of the triangulated shear model used to illustrate Extensional fault-propagation fold, modified from Nabavi and Fossen (2021).

https://doi.org/10.5194/nhess-2024-170
Preprint. Discussion started: 5 March 2025

Natural Hazards and Earth System Sciences
Discussions

4. Results

4.1 Features of active tectonic on the N9 reflection seismic profile

This study primarily investigated the dislocation and deformation properties of the sedimentary layer, as well as its interactions with the underlying basement. The offshore of Nan'ao is divided into two regions based on their geological composition. The northwest region consists of an old Paleoproterozoic basement, while the southeast region is defined by a Mesozoic basement (Yang, 2015). These findings indicate that the tectonic activity in the southeastern study area may have been affected by subsequent magmatic activities. In addition, the basement in the southeast is comparatively shallow, with certain regions even revealing the surface of the seabed. Effective information on tectonic activity in the southeast is significantly reduced by the characteristic indistinctness of igneous rocks in seismic data. A certain sedimentary layer close to the LF are retained in the data gathered from the N9 profile.

Two separate basement faults, designated F1 and F2, are found in the W9 profile (Fig. 4c). At the tip of fault F1, the sedimentary layer in the sparker profile N9 show signs of recent activity. A feature of extensional fault propagation folds, an upward-expanding deformation zone is seen at the top end of fault F1, where internal strata progressively form broad monoclinal folds (Fig. 4b). This represents the most recent activity of fault F1 and manifests as a topographic step up to 10 km wide on the seafloor (Fig. 4b). Moreover, fault F1 is located in the same place as seismic cluster zones and the previously established position of the LF (Figs. 1 and 2). This allows us to confirm that fault F1 is indeed the previously identified LF. On the other hand, fault F2 (Fig. 4c) stretches from the shallow sedimentary layers to the bottom in a faulted way (Fig. 4b), indicative of active growth faulting (Fig. 4d). What is the reason for the significant difference in recent activity between these two basement faults in the shallow sedimentary layers? We believe this is determined by the mode of fault movement, where shallow structural features carry the kinematic characteristics of deeper fault activity.

https://doi.org/10.5194/nhess-2024-170
Preprint. Discussion started: 5 March 2025

Natural Hazards and Earth System Sciences
Discussions

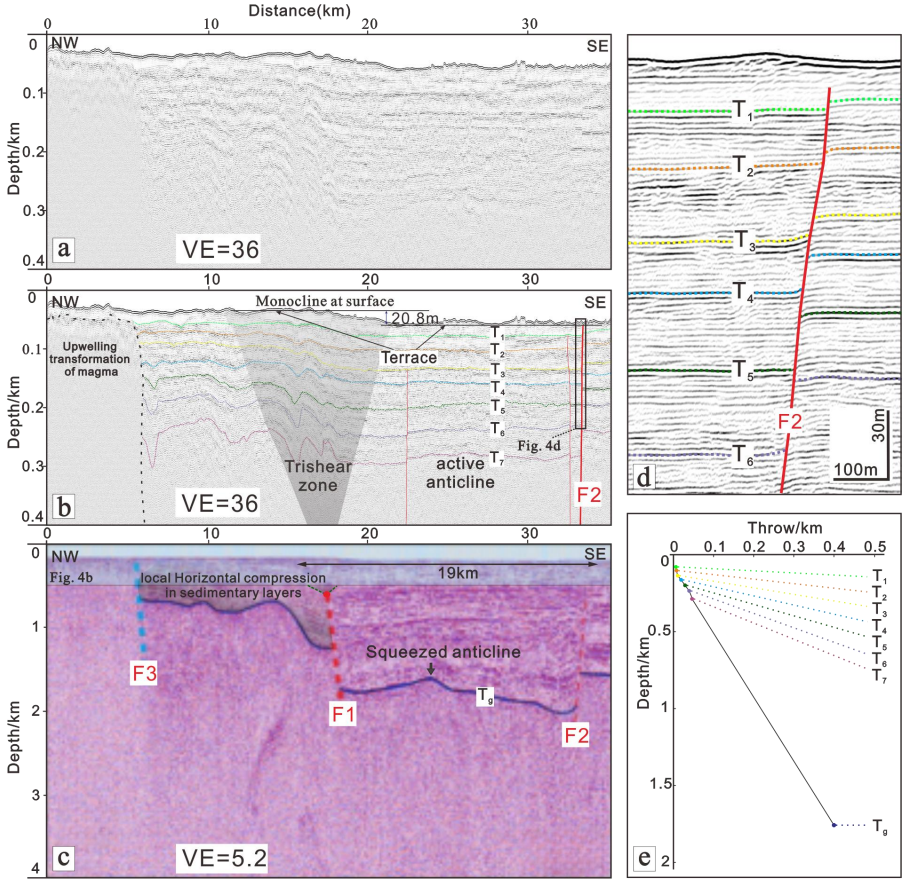

Figure 4. (a) Sparker reflection seismic profile N9 off Nan'ao (profile location shown in Fig. (2); (b) Interpretation of sparker profile N9 off Nan'ao. It reveals a topographic terrace at the location of fault F1 on the seabed, with the shallow sedimentary layer below Showing monoclinal fold deformation. The trishear zone marked (light gray fill) indicates the range of influence of reactivated basement normal faulting, with compressional folding present in the footwall strata of fault F1; (c) G gun reflection seismic profile W9 off Nan'ao (modified from Xia et al. (2020), profile location shown in Fig. 2. It can be nested with profile N9 for interpretation longitudinally, with blue translucent range corresponding to profile N9; (d) Fault F2 as a typical growth fault, linearly cutting to the seabed; (e) T-Z plot of fault F2 shows that over a considerable period of time until present, fault F2 has been consistently active in a similar manner and nearly constant rate.

4.2 Latest activity of shallow structure

We performed a statistical study to measure the level of activity of faults and folds by examining the link between fault throw/fold amplitude and depth. The subjects under examination encompass monocline folds (depicted in Figs. 4b and 5), compressional folds (shown in Figs. 4b and 6) within the

https://doi.org/10.5194/nhess-2024-170
Preprint. Discussion started: 5 March 2025

Natural Hazards and Earth System Sciences
Discussions
Open Access
EGU

trishear zone located above the main fault F1, and the antithetic fault F2 (shown in Figs. 4b and 4d). The strata located inside the trishear zone above fault F1 experience both compressive and extensional stresses. To mitigate the compressive effect, we have rebuilt the strata accordingly (Figs. 5 and 6).

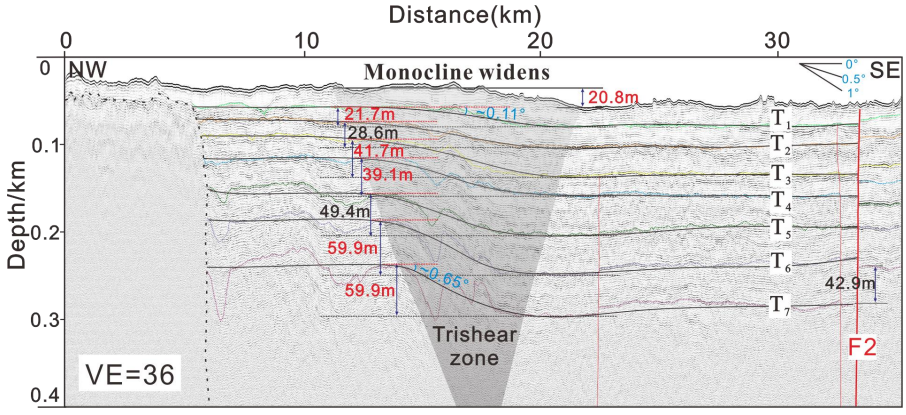

Figure 5. Monoclinal folds amplitude on profile N9 (profile location shown in Fig. 1). We conducted certain restorations of the strata; the black lines depict the strata unaffected by compression, aimed at reconstructing the true form of the monoclinal folds. No changes in monoclinal fold morphology were observed during periods T7 to T6, T4 to T3, and T1 to seabed. The amplitudes of monoclinal folds during these three periods form an arithmetic sequence, with a difference of approximately 20 m. This suggests that each stress release after accumulation causes a total drop of about 20 m. If this release matches the accumulation, it implies that the stress accumulated by fault F1 each time it reaches active conditions needs to reach a fixed threshold.

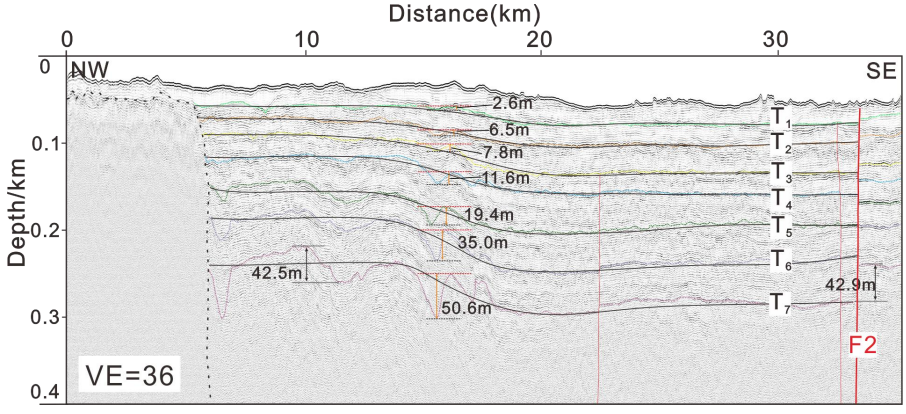

Figure 6. Compression folds amplitude in the footwall of fault F1 on profile N9. Due to the influence of monocline folding, it is difficult to select horizontal lines, so we choose to measure "wave height" to indicate the degree of compressional fold.

https://doi.org/10.5194/nhess-2024-170
Preprint. Discussion started: 5 March 2025

Natural Hazards and Earth System Sciences
Discussions

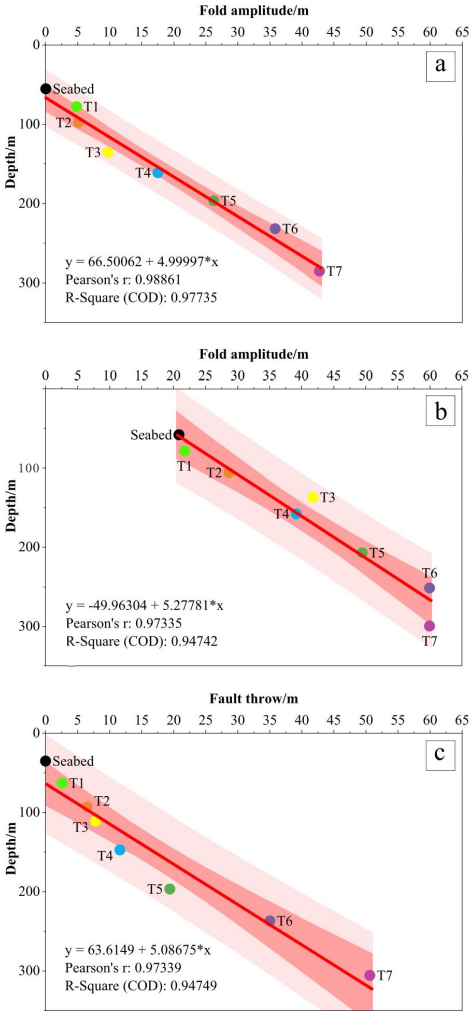

Figure 7. Correspondence between fault throw/fold amplitude and depth on profile N9 (with the best-fit regression and correlation coefficient R2 provided). Analyzed features include: (a) compression folds in the footwall of fault F1; (b) monoclinal folds formed above the break point of fault F1; (c) antithetic fault F2 in the hanging wall of fault F1.

5. Analysis

5.1 The regularity of superficial structural activities

Using a structural framework, we tried to understand and characterize the general tectonic movements of the research region. Faults F1 and F2 relative slide create a substantial graben wedge that can span up to 19 km. A compensatory squeezed anticline exists between the two faults (Fig. 4c), and A slight

https://doi.org/10.5194/nhess-2024-170
Preprint. Discussion started: 5 March 2025


Natural Hazards and Earth System Sciences
Discussions

active anticline is also observed in the overlying sedimentary layer above the basement anticline (Fig. 4b). Simultaneously, the footwall of fault F1 displays a gradual increase in compressional folding, starting from the sedimentary layer and extending to the basement (Fig. 4b), these folds are a result of the lateral compression exerted by the hanging-wall wedge of fault F1 during the processes of tilting and sliding. Various components of this architectural framework have distinct and unique structural characteristics. To ascertain whether these disparities are indicative of how this structural system moves to a certain degree, more validation is required by correlating the identified active structures.

Several key geological structural patterns were identified through the analysis. Firstly, three different structural phenomena exhibit similar activity patterns over the same period, persisting with their respective unique movement modes and relatively stable rates until present (Fig. 7). Secondly, monoclinal folds exhibit the largest amplitude (Fig. 7b), reflecting their dominant role in the activity of the study area. Additionally, unlike the other two persistent structural phenomena, activity analysis indicates periods of inactivity for monoclinal folds (Fig. 7b). Finally, the antithetic fault in the hanging-wall and compressional folds in the footwall show more consistent activity intensity and rate (Figs. 7a and 7c), further confirming our initial hypothesis: the activity of the antithetic fault represents the movement characteristics of the graben block, while the compressional folds are associated products of this movement process, demonstrating the causality between the two.

5.2 Forward modeling of F1 fault-propagation fold

Withjack (1990) simulated the phenomenon where normal faulting at the basement generates monoclinal folds at the surface (Fig. 3c). At the top of the basement fault, there is a deformational zone that widens upwards, and the hanging-wall transmits the vertical displacement of basement fault slip in the form of monoclinal folds (Fig. 3d). The activity of fault F1 in this study serves as a typical natural example, where a terrain terrace on the seafloor up to 10 km wide may directly correspond to basement normal faulting. Additionally, the results of the activity analysis indicate that the activity of fault F1 exhibits a characteristic of periodic behavior (Fig. 7b).

It is clear from Fig. 7b that there is a distinct signal of "activity cessation" in the association between monoclinal folding and depth for the strata of T7 to T6, T4 to T3, and T1 to the seafloor. The amplitude values of the monoclinal fold throughout these three times form an arithmetic sequence with a difference of roughly 20 m. Notably, the current seafloor at the F1 fault location also shows a drop of

https://doi.org/10.5194/nhess-2024-170
Preprint. Discussion started: 5 March 2025


Natural Hazards and Earth System Sciences
Discussions

about 20 m, and the 59.9 m vertical displacement at the T7 interface is attributed to the rapid activity across three periods, which occurred after the formation of the T6 interface, the T3 interface, and the present seafloor. To support our argument, we employed the trishear numerical modelling **FaultFold V7** (Allmendinger, 1998) was used to simulate the deformation process of fault F1(Fig. 8). The model incorporates layer thickness and slip distances derived from depth-converted seismic profiles (Fig. 5). The dip angle of the main fault is established at 75°, relying upon prior research (Deng, 2019). The apex angle of the trishear model is set at 50° to regulate the strain range above the fault, without any inherent physical significance, but rather based on the aspect ratio of Fig. 5. The N9 profile (Figs 4b and 5) shows that the fault does not propagate into the sedimentary layers, and the P/S ratio is set to 0 for simplicity.

In the resulting model of Fig. 8, The dynamic evolution of the recent activities of fault F1 in the model depicted can be elucidated by a 5-step model, which delineates 3 phases of rapid activity interspersed with 2 comparatively longer periods of quiescence. The seabed in steps b, d, and f exhibits abrupt development of seafloor terraces, which are understood as the reactivation of the underlying fault. The vertical displacement of the monoclinal fold at the T7 interface is 59.9 m, and the overall displacement from the three periods of fault activity equals 59.9 m. This indicates that the "growth strata" phase in the model does not cause additional displacements, which corresponds to a period of quiescence. The "activity" of the strata is demonstrated by the thickness of the hanging wall under differential subsidence in later phases, which is a result of the relatively quick sliding during the fault activity periods increasing accommodation space for the hanging wall. Using the expansion index analysis to interpret fault activity might lead to misjudgment (Jackson et al., 2016). The forward modeling demonstrates the process and patterns of fault F1's activity. The model results (Fig. 8f) are consistent with the real data (Fig. 7b). However, the conclusion is that fault F1 did not show synsedimentary activity, but rather experienced seismic-scale strain.

https://doi.org/10.5194/nhess-2024-170
Preprint. Discussion started: 5 March 2025

Natural Hazards and Earth System Sciences
Discussions
Open Access
EGU

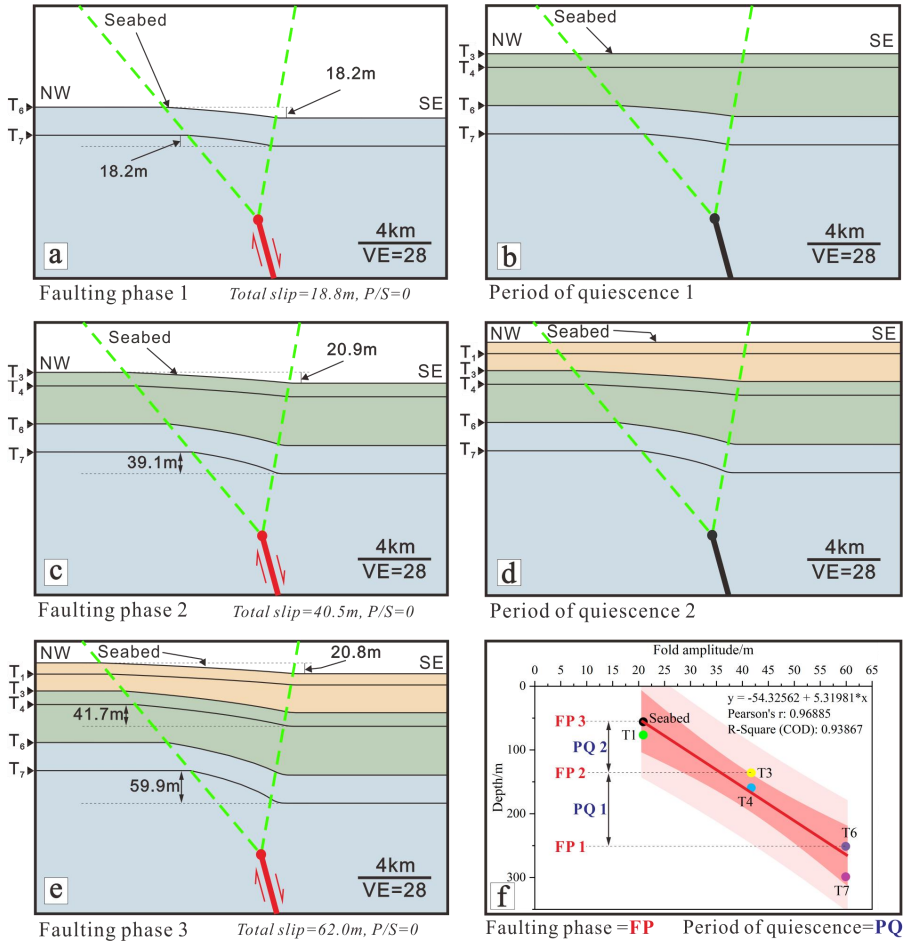

315

Figure 8. Forward modeling of extensional fault propagation folds at the tip of fault F1. Panels (a)–(e) show the evolution steps of the shallow sedimentary layers of fault F1 using the FaultFold V7 modeling software. Panel (f) shows the correspondence between the monoclinal fold amplitude and depth at the tip of the the fault F1, which represents the evolution to the present time (step e).

320 ## 6. Discussion

In general, this article discusses several closely related issues: (1) What structural features and kinematic processes may high-resolution reflection seismic data disclose about the study area today? (2) What insights might the quantitative study of superficial activities bring for deeper activities? (3) What direct connections exist between the revealed tectonic activities and earthquakes/tsunamis in the study

325 area?

https://doi.org/10.5194/nhess-2024-170
Preprint. Discussion started: 5 March 2025


Natural Hazards and Earth System Sciences
Discussions

6.1 Evidence of F1 shallow strata deformation connected to the 1918 Nan'ao earthquake

The geometric shapes and kinematic features of shallow structures can be obtained from high-resolution reflection seismic data. Our study reveals the latest activities of two basement normal faults, F1 and F2. Previous analyses indicate that unlike the continuous activity of growth fault F2, fault F1 experiences long periods of dormancy and brief periods of activity, corresponding to long-term stress accumulation and rapid energy release during seismic cycles. Fault F1 precisely aligns with the previously identified LF (Figs 1 and 2), which is considered the main seismogenic fault of the 1918 Nan'ao M7.3 earthquake in the study area(Liu, 1985; Xu et al., 2006; Xia et al., 2020). Xu et al. (2006) analyzed the seismic intensity, distribution of earthquake intensity zones, and seismic source structure of the 1918 Nan'ao earthquake, and located its epicenter approximately 6 km southeast of Nanpeng Islands in the sea, coordinates 23.2°N, 117.3°E (Figs 1, 2 and 3), with a depth of 15 km. Spatially, this location coincides with the extension below fault F1. Therefore, fault F1 is highly likely to be the co-seismic fault of the 1918 Nan'ao M7.3 earthquake. Our survey data show that faults F1 and F2 affect the seabed through folding deformation and fault cutting, respectively, both results of basement normal fault activities. Shallow data indicate that the structural phenomena occur in a single active mode without evidence of later inversion, suggesting that the ongoing normal fault activities represent the current tectonic movement mode in the research region. We attempt to further understand the relationship between the shallow fault activity mode in the research region and the occurrence of the 1918 Nan'ao M7.3 earthquake as well as its associated "draw-down" tsunami.

6.2 Normal faulting activity in the Nan'ao offshore and graviquakes

The 1994 M7.3 earthquake, which occurred along a normal fault in the Taiwan Strait (Fig 1), is the most significant seismic event detected by contemporary seismic monitoring in the vicinity of the research region. In the same structural stress circumstances in the area, the geometry characteristics of the seismogenic fault Yizhu fault (Fig 1) is similar to that of the LF in the Taiwan Strait (Wang et al., 2011). Considering the latest normal fault activities discovered in this investigation, we will explore whether the 1918 Nan'ao M7.3 earthquake was also a normal fault event. Based on the shallow fault movement characteristics found in this study, we can draw insights from studies of normal fault earthquakes in other regions across the globe that have extensive seismic monitoring data available. Bignami et al. (2019) discussed two competing models for brittle upper crustal deformation related to

https://doi.org/10.5194/nhess-2024-170
Preprint. Discussion started: 5 March 2025

normal fault earthquakes: the elastic rebound model and the gravitational collapse model (Fig. 9), and they believed that the gravitational collapse model is more consistent with the actual observation results. Different fault system movements imply differences in energy accumulation and release mechanisms. Many scholars suggest that, unlike earthquakes generated by thrust and strike-slip faults fueled by elastic energy, normal fault earthquakes mainly release gravitational potential energy (Doglioni et al., 2015, 2014; Petricca et al., 2015; Savage and Walsh, 1978; Albano et al., 2021a; Albano et al., 2021b; Muldashev et al., 2022; Petricca et al., 2021), In the gravitational collapse model, faults penetrating the crust exhibit episodic locking-unlocking behavior in the brittle upper crust (Carminati et al., 2020), similar to the active behavior of the main fault F1 observed in shallow sediments in this study. This model also hypothesizes the development of an expanding wedge that may evolve into a normal fault, while our investigation seems to have directly identified the existence of this antithetic normal fault, namely fault F2, and explains its current activity status.

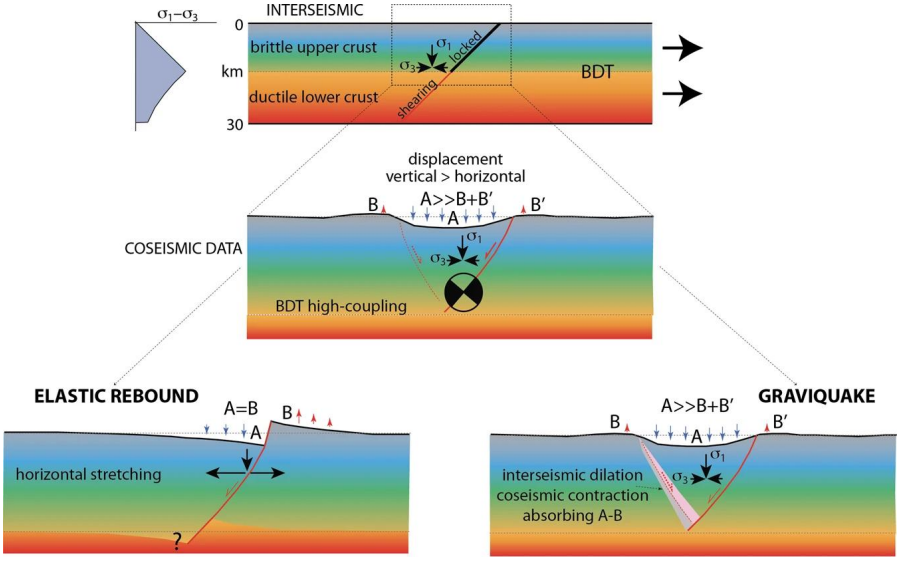

Figure 9. A comparison of two modes that explain earthquake occurrences linked to normal faults. Elastic rebound activation caused by crustal extension (lower left figure) or activation due to gravitational collapse of the hanging wall (lower right figure), quoted from Bignami et al. (2019). According to current understanding, the LF is a normal fault activity that inclines to the southeast and reaches the moho surface, and the tensile fracture has stopped at present. Current extensional activity is difficult to explain with horizontal crustal stretching.

Doglioni et al. (2015) and Petricca et al. (2015) referred to earthquakes that release gravitational

https://doi.org/10.5194/nhess-2024-170
Preprint. Discussion started: 5 March 2025

potential energy as graviquakes. The magnitude of graviquakes mainly depends on the mass/volume involved in the coseismic collapse phase (Petricca et al., 2015; Bignami et al., 2020). Studies suggest that an increase in the depth of the brittle-ductile transition zone and the length of faults (with an average depth-to-length ratio of 3±1) determines an increase in the volume involved during earthquakes, thereby increasing earthquake magnitude. According to the BDT 15km deep model calculated by Bignami et al. (2020), gravity-driven normal slip can cause earthquakes up to a maximum magnitude of M_w7.2, equivalent to the Nan'ao M7.3 earthquake in 1918. The importance of the volume of blocks involved in earthquakes can be supported by the results of this observation. In the current tectonic activity system, gravitational effects come from the weight of wedge-shaped blocks hanging above faults F1 and F2, with the volume of the wedge relatively constant. Therefore, the accumulated energy and release threshold should be relatively constant values (Figure 10b). The seabed drop caused by each activation period of fault F1 is relatively stable, around 20 m each time (Figs. 8a, 8c, 8e). With an increase of the load on the hanging-wall, the accumulated energy and maximum principal stress increase, shortening the time required to reach the sliding critical point (Fig. 10c). The second period of quiescence shown in simulation results is shorter than the first (PQ2<PQ1) (Fig. 8f). In addition, we found slight differences in seabed drops caused by the three periods of activity. According to the explanation of gravitational seismic patterns (Petricca et al., 2015), with an increase in load, the total seabed drop caused by each period of activity should show an increasing trend. Data results show that the seabed drop caused by the Faulting phase 2 is greater than that caused by the Faulting phase 1, but is similar to the current seabed drop, suggesting that the current period of activity may has not yet ended. The active seismic background in the offshore of Nan'ao of the LF seems to support this. We have reason to assume that the normal fault activities in the offshore of Nan'ao are related to the gravitational effect of the wedge-shaped block above fault F1.

A ductile layer of a certain thickness exists in the crust of the South China continental margin at a depth of about 10–25km (Wang, 2001; Zhou et al., 2004; Cao et al., 2018; Li et al., 2023). Previous studies using wide-angle seismic surveys revealed the crustal structure in the transition zone between sea and land in the offshore of Nan'ao, identifying weak zones and local low-velocity zones in the crust (Xia et al., 2020; Zhao et al., 2004). Line N9 mostly demonstrates high-velocity anomalies at depths of 20 and 25 km, whereas low-velocity anomalies have been observed at depths of 10 and 15 km (Xia et al.,

https://doi.org/10.5194/nhess-2024-170
Preprint. Discussion started: 5 March 2025


Natural Hazards and Earth System Sciences
Discussions

2020). The mechanical property differences between weak interlayers and adjacent layers are similar to some experimental simulations, which may help explain the formation of antithetic faults at depth. For instance, Holland et al. (2011) reproduced the formation of antithetic faults in physical simulations of normal fault propagation using wet sand as a plastic material, and Hardy (2018) demonstrated the development of antithetic faults in discrete element numerical simulations based on the normal fault propagation in friction-cohesion covered area. Therefore, the appearance of antithetic fault events may be caused by variations in rheology with underlying formations and the rheological properties of local crustal weak layers.

In previous normal fault seismic models, the expansion and compression of the conjugate wedge correspond to the accumulation and release of energy (Fig. 9). The hypothesis of the conjugate weak zone is more inferred based on the distribution of seismic events and the movement mode of fault systems. Our research combines the deep geological structure of the offshore of Nan'ao with the shallow active features of antithetic faults to offer an alternative explanation for the creation of gravity gradients. For wedge-shaped blocks confined by two opposite faults, the current overall compressive environment favors maintaining their stable state. In this scenario, gravity becomes the primary force governing their movement. However, why does omnipresent gravity cause differential movements on both sides of graben blocks? To tackle this problem, we present the notion of shear stress and material attributes. Under conditions of high-angle shearing, materials are less inclined to undergo brittle failure until they undergo brittle fracture under normal stress. Conversely, under conditions of low-angle shearing, materials are more susceptible to sliding and plastic deformation. The intersection angle of main fault F1 or antithetic fault F2 with the ductile interlayer corresponds precisely to this mechanism. The dip angle of the main fault F1, ranging from 70 to 80°, almost vertically penetrates to the moho interface, while the dip angle of the antithetic fault measures approximately 60° in the shallow sedimentary layer and decreases further with depth. Seismic profile data indicate sustained and relatively uniform activity of the antithetic fault (Figs. 4e and 7c). During interseismic periods, we believe the antithetic fault causes continuous plastic deformation at the interface with the plastic layer under low-angle shear stress, providing necessary strain space for downward sliding. The activities of the antithetic fault causes the hanging-wall wedge of the main fault to squeeze one side of the footwall (Fig.s 4b and 4c), potentially pushing material from weak layers into the footwall of the main fault F1, causing the uplift of footwall. In this process, the confining pressure of the wedge-shaped block

https://doi.org/10.5194/nhess-2024-170
Preprint. Discussion started: 5 March 2025

Natural Hazards and Earth System Sciences
Discussions
Open Access
EGU

decreases, reducing the minimum stress (σ3), thereby increasing differential stress during interseismic periods, enlarging the left-lateral Mohr circle. Once the equilibrium is disrupted, it marks the beginning of coseismic periods (i.e., tectonic active periods), until the accumulated stress gradient between the inactive upper crust segment and the active ductile layer is fully released. Once the hanging-wall wedge stabilizes, a new cycle of stress accumulation begins, re-entering an interseismic period (Fig. 10a).

Bounded by Fault F1 (LF), the shore side is studded with islands, and the seaward side is flat. Since the beginning of neotectonics, the coastal areas of Zhejiang and Fujian have experienced a general elevation, with contour lines showing changes that run parallel to the direction of LF, which tend northeastward. Within the southeastern coastal regions, particularly in southern Fujian and eastern Guangdong, there is a prevalent circulation of popular sayings like "Dongjing sinks, Fujian rises" or "Dongjing sinks, Nan'ao rises". It is believed that the vanished "Dongjing" was situated in waters between 30 m and 50 m deep close to the Nanpeng Islands (Zhan et al., 2002). This reflects the geological uplift and subsidence that has occurred in the research area over the previous millennium, consistent with the activity patterns reflected by the movement modes.

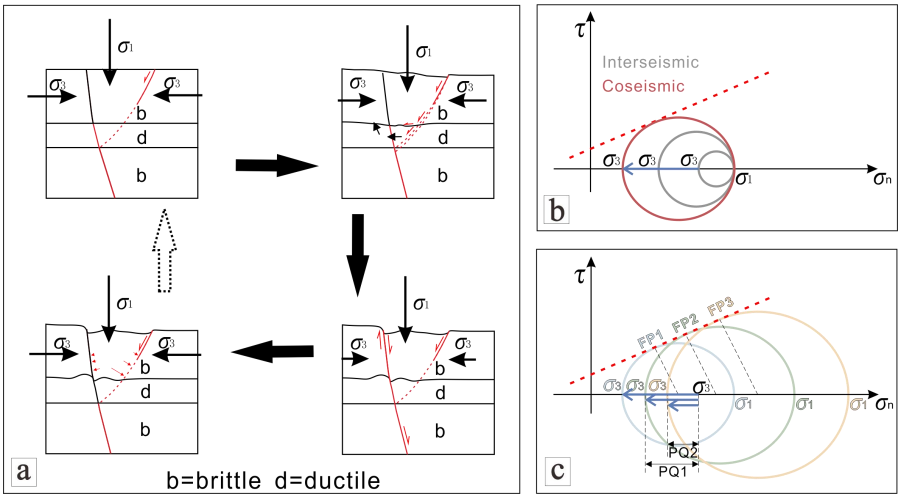

https://doi.org/10.5194/nhess-2024-170
Preprint. Discussion started: 5 March 2025

Figure 10. panel (a) describes the repeated nucleation process of earthquakes corresponding to this study. It is important to note that in the gravity seismic model described in this paper, the wedge-shaped bodies include a ductile layer, where the antithetic fault continues downward sliding during interseismic periods. It is presumed that this movement causes plastic deformation in the ductile layer and pushes the weak layer into the footwall, reducing confining pressure, and thus continuously decreasing σ3 (horizontal direction) until reaching the critical imbalance threshold to enter the coseismic phase. This model also corresponds to the asymmetric half-graben basin in the Taiwan Strait. In panel (b), the Mohr diagram illustrates the evolution of stress states during interseismic (gray circle) and coseismic (red circle) periods, adapted from Carminati et al. (2020). In panel (c), the Mohr circle shows that with increasing load, the cycle of earthquake recurrence shortens, while energy release increases.

6.3 Coseismic deformation model

After analyzing the movement modes existing in this tectonic system, this study constructs a coseismic deformation model based on actual proportions (Fig. 11). In this fault system, fault F1 is an active fault penetrating the entire crust, appearing locked in brittle upper crust and with constant strain rate in its antithetic fault (Fig. 11). After instability of fault F1, a long period is required to regain stress balance, with its upward deformation gradually absorbed by shallow layers, which can be illustrated through the propagation folds of normal faults. The hanging-wall wedge block of fault F2 experiences only gravitational collapse, directly faulting the seabed, making its activity easier to reach equilibrium. In model Fig. 11, fault F3 is inferred from the role of the ductile layer during fault activity. As faults propagate into the ductile layer, vertical forces gradually convert into tension on one side of the footwall, leading to bending and sliding folds, which may produce two effects: (1) stretching characteristics exhibited in folding actions; (2) along-layer shear adjustment effect (Ferrill et al., 2007; Deckers, 2015), indicating decoupling of layers. These effects provide space for activity of F3, which is depicted as a large detachment fault converging within the ductile layer in the model. According to the elastic dislocation theory in an extensional environment (Okada, 1985), the appearance of the Lemen Islands may be related to the activity of this detachment fault, while the appearance of the Nanpeng Islands is related to the normal fault activities of F1.

https://doi.org/10.5194/nhess-2024-170
Preprint. Discussion started: 5 March 2025

Natural Hazards and Earth System Sciences
Discussions

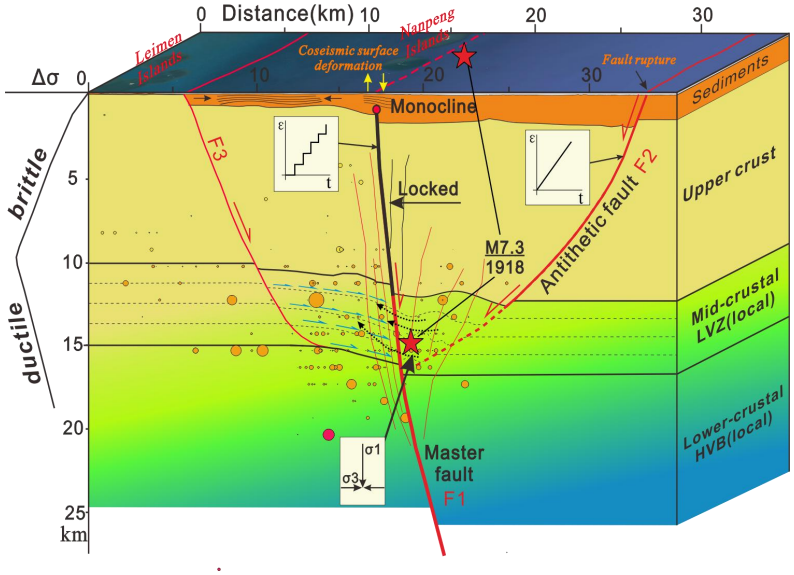

Figure 11. Normal fault activity model in the LF in the offshore of Nan'ao. The shallow cross-section is constructed based on data from reflection seismic profiles N9 and W9. Two red pentagram stars on the figure indicate the projection positions on profile N9 and the horizontal plane of the 1918 M7.3 earthquake. The location is based on Xu et al. (2006). The deep structure is based on Wang (2001), Xia et al. (2020) and Zhou et al. (2004). Small circles represent seismic events (2018–2023) occurring 9 km on either side of N9 line, vertically projected on profile N9, sourced from the Fujian Earthquake Agency. Red single-sided arrows indicate fault slip direction; blue single-sided arrows indicate interlayer slip direction; thin black dashed arrows indicate the direction in which soft matters are extruded.

6.4 Seismic patterns indicative of tsunami activity

Earthquakes need to produce a rapid seafloor drop to trigger tsunamis. Explaining the 1918 Nan'ao earthquake-induced tsunami using the strike-slip activity of the LF is a difficult task. Superficial structure morphology can reflect deeper activities to some extent. We can also rely on models such as the trishear model simulating the propagation of extensional fault folds to address this issue. In this model (Fig 3c), the ratio of fault propagation amount to slip amount (p/s) reflects the relative instantaneous rate at which the fault endpoint propagates upward within geological bodies, determining the deformation outcomes of basement fault activities in the sedimentary layer. If the p/s value is sufficiently large, the strata only exhibit slight deformation or are directly cut by faults without deformation occurring (Jin and Groshong, 2006). In this study, a p/s value of 0 is assigned, and the simulation results correspond well with actual profiles (Fig. 8). At the main fault F1 location, the vertical drop caused by the main earthquake is absorbed by a 10 km-wide seabed gentle slope (~0.1°).

https://doi.org/10.5194/nhess-2024-170
Preprint. Discussion started: 5 March 2025


Natural Hazards and Earth System Sciences
Discussions

Clearly, there is no seabed faulting at the main fault location, but in the same sedimentary layer, the antithetic fault cuts sharply to the seabed. We believe that the antithetic fault F2 slides faster than F1 at the shallow layer, causing rapid seabed faulting at the F2 location. According to historical records, during the Nan'ao earthquake on February 13, 1918, a ship docked at Shantou pier had its bottom actually touching the seabed, with "tidal recession and resurgence," and "surging seawater," indicating a pronounced descending-type tsunami caused by earthquakes. The activity energy of the antithetic fault F2 discovered in this study corresponds to the phenomena: seabed faulting, tilting towards the continental normal fault, parallel to the coastline, and occurring at a deeper position than the main fault, allowing it to encompass more seawater during activity. Hence, we consider the rapid sliding of the antithetic fault F2, accompanied by the collapse of a 19 km-wide graben, as the cause of destructive tsunamis, rendering it an essential component of the seismic framework of the offshore of Nan'ao.

7. Conclusions

In this study, we obtained the data of the seabed topography and near-seabed strata in the LFZ in the offshore of Nan'ao by using the seismic method of high-resolution marine sparker source mini-multichannel reflection seismic to explore its latest activities. Unlike previous studies focusing mainly on its strike-slip characteristics, this study explores its kinematic processes and investigates the relationship between normal oblique slip and seismic activities based on recently observed active normal faulting morphology and establishes a model for normal fault earthquakes. We believe that the release of gravitational potential energy from the hanging-wall wedge block during normal oblique slip of fault F1 can produce an M7.2 earthquake, corresponding to the 1918 M7.3 earthquake in Nan'ao, and explains the descending-type tsunami triggered by the 1918 Nan'ao earthquake using this normal fault earthquake model.

The introduction of the normal fault earthquake model requires a reassessment of seismic and tsunami risks caused by LF in future studies. The assessment of normal fault earthquakes is distinct from that of strike-slip earthquakes. In the case of normal fault earthquakes, the focus is on the intensity of the rock's yield stress (including factors such as upper crust thickness, bending, and squeezing). On the other hand, strike-slip earthquakes consider more of the length and magnitude of faults. Moreover, considering the kinematic characteristics of LF propagating upwards, refining surface structural

https://doi.org/10.5194/nhess-2024-170
Preprint. Discussion started: 5 March 2025

analysis to deduce deep-seated activities will help us understand more accurately the interactions between deep processes and surface responses.

CRedit authorship contribution statement

Hu Yi: Conceptualization, Data curation, Formal analysis, Investigation, Methodology, Software, Validation, Writing - original draft. **Wenhuan Zhan:** Methodology, Project administration. **Jian Li:** Writing - review & editing, Funding acquisition. **Xiaochuan Wu:** Conceptualization, Methodology. **Xiaodong Yang:** Conceptualization, Methodology. **Jie Sun:** Project administration, Supervision. **Yantao Yao:** Writing - review & editing. **Jiaxian Huang:** Visualization. **Zelong Ju:** Visualization.

Declaration of Competing Interest

This manuscript has not been published or presented elsewhere in part or in entirety and is not under consideration by another journal. We have read and understood your journal's policies, and we believe that neither the manuscript nor the study violates any of these. There are no conflicts of interest to declare.

Data availability

Data will be made available on request.

Acknowledgements

This research was jointly supported by the National Key R&D Program of China (No. 2022YFC3103800), National Natural Science Foundation of China (Nos. 42206069 and 41876067), and Science and Technology Projects of Guangzhou (No. 2023A04J0191).

References

Albano, M., Barba, S., Bignami, C., Carminati, E., Doglioni, C., Moro, M., Stramondo, S., and Saroli, M.: Three-dimensional numerical simulation of the interseismic and coseismic phases associated with the 6 April 2009, Mw 6.3 L'Aquila earthquake (Central Italy), Tectonophysics, 798, 228685, https://doi.org/10.1016/j.tecto.2020.228685, 2021a.

https://doi.org/10.5194/nhess-2024-170
Preprint. Discussion started: 5 March 2025

Natural Hazards and Earth System Sciences
Discussions

Albano, M., Barba, S., Bignami, C., Carminati, E., Doglioni, C., Moro, M., Saroli, M., Samsonov, S., and Stramondo, S.: Numerical analysis of interseismic, coseismic and post-seismic phases for normal and reverse faulting earthquakes in Italy, Geophysical Journal International, 225, 627-645, https://doi.org/10.1093/gji/ggaa608, 2021b.

Allmendinger, R. W.: Inverse and forward numerical modeling of trishear fault-propagation folds, Tectonics, 17, 640-656, https://doi.org/10.1029/98tc01907, 1998.

Allmendinger, R. W. and Shaw, J. H.: Estimation of fault propagation distance from fold shape: Implications for earthquake hazard assessment, Geology, 28, 1099-1102, https://doi.org/10.1130/0091-7613(2000)28<1099:Eofpdf>2.0.Co;2, 2000.

Bignami, C., Valerio, E., Carminati, E., Doglioni, C., Petricca, P., Tizzani, P., and Lanari, R.: Are normal fault earthquakes due to elastic rebound or gravitational collapse?, Annals of Geophysics, 63, 1–15, https://doi.org/10.4401/ag-8455, 2020.

Cao, J. H., Xia, S. H., Sun, J. L., Zhao, F., Wan, K. Y., and Xu, H. L.: Offshore Fault Geometrics in the Pearl River Estuary, Southeastern China: Evidence from Seismic Reflection Data, Journal of Ocean University of China, 17, 799-810, https://doi.org/10.1007/s11802-018-3499-5, 2018.

Carminati, E., Bignami, C., Doglioni, C., and Smeraglia, L.: Lithological control on multiple surface ruptures during the 2016-2017 Amatrice-Norcia seismic sequence, Journal of Geodynamics, 134, 101676, https://doi.org/10.1016/j.jog.2019.101676, 2020.

Charvet, J., Lapierre, H., and Yu, Y.: Geodynamic significance of the Mesozoic volcanism of southeastern China, Journal of Southeast Asian Earth Sciences, 9, 387-396, https://doi.org/10.1016/0743-9547(94)90050-7, 1994.

Chou, Y. W. and Yu, H. S.: Structural expressions of flexural extension in the arc-continent collisional foredeep of western Taiwan, Geological Society of America Special Paper, 358, 1-12, https://doi.org/10.1130/0-8137-2358-2.1, 2002.

Coleman, A. J., Duffy, O. B., and Jackson, C. A. L.: Growth folds above propagating normal faults, Earth-Science Reviews, 196, 102885, https://doi.org/10.1016/j.earscirev.2019.102885, 2019.

Deckers, J.: Decoupled extensional faulting and forced folding in the southern part of the Roer Valley Graben, Belgium, Journal of Structural Geology, 81, 125-134, https://doi.org/10.1016/j.jsg.2015.08.007, 2015.

Deng, K.: Tectonic characteristics of the Binhai Fault Zone in Taiwan Strait, Marine Geology & Quaternary Geology, 39, 72-80, https://doi.org/10.16562/j.cnki.0256-1492.2019081301, 2019.

Doglioni, C., Barba, S., Carminati, E., and Riguzzi, F.: Fault on-off versus coseismic fluids reaction, Geoscience Frontiers, 5, 767-780, https://doi.org/10.1016/j.gsf.2013.08.004, 2014.

Doglioni, C., Barba, S., Carminati, E., and Riguzzi, F.: Fault on-off versus strain rate and earthquakes energy, Geoscience Frontiers, 6, 265-276, https://doi.org/10.1016/j.gsf.2013.12.007, 2015.

Erslev, E. A.: Trishear fault-propagation folding, Geology, 19, 617-620, https://doi.org/10.1130/0091-7613(1991)019<0617:Tfpf>2.3.Co;2, 1991.

Ferrill, D. A., Morris, A. P., and Smart, K. J.: Stratigraphic control on extensional fault propagation folding: Big Brushy Canyon monocline, Sierra Del Carmen, Texas, Geological Society London Special Publications, 292, 203-217, https://doi.org/doi:10.1144/SP292.12, 2007.

Grützner, C., Carson, E., Walker, R. T., Rhodes, E. J., Mukambayev, A., Mackenzie, D., Elliott, J. R., Campbell, G., and Abdrakhmatov, K.: Assessing the activity of faults in continental interiors: Palaeoseismic insights from SE Kazakhstan, Earth and Planetary Science Letters, 459, 93-104, https://doi.org/10.1016/j.epsl.2016.11.025, 2017.

https://doi.org/10.5194/nhess-2024-170
Preprint. Discussion started: 5 March 2025

Hardy, S. and Ford, M.: Numerical modeling of trishear fault propagation folding, Tectonics, 16, 841-854, https://doi.org/10.1029/97TC01171, 1997.

Hardy, S. and McClay, K.: Kinematic modelling of extensional fault-propagation folding, Journal of Structural Geology, 21, 695-702, https://doi.org/10.1016/s0191-8141(99)00072-3, 1999.

Jackson, C., Bell, R., Rotevatn, A., and Tvedt, A.: Techniques to determine the kinematics of synsedimentary normal faults and implications for fault growth models, Geological Society London Special Publications, 439, https://doi.org/10.1144/SP439.22, 2016.

Jin, G. H. and Groshong, R. H.: Trishear kinematic modeling of extensional fault-propagation folding, Journal of Structural Geology, 28, 170-183, https://doi.org/10.1016/j.jsg.2005.09.003, 2006.

Julve, J., Barbot, S., Moreno, M., Tassara, A., Araya, R., Catalan, N., Crempien, J. G. F., and Becerra-Carreno, V.: Recurrence time and size of Chilean earthquakes influenced by geological structure, Nature Geoscience, 17, https://doi.org/10.1038/s41561-023-01327-8, 2024.

La Bruna, V., Agosta, F., Lamarche, J., Viseur, S., and Prosser, G.: Fault growth mechanisms and scaling properties in foreland basin system: The case study of Monte Alpi, Southern Apennines, Italy, Journal of Structural Geology, 116, 94-113, https://doi.org/10.1016/j.jsg.2018.08.009, 2018.

Li, J. H., Dong, S. W., Cawood, P. A., Thybo, H., Clift, P. D., Johnston, S. T., Zhao, G. C., and Zhang, Y. Q.: Cretaceous long-distance lithospheric extension and surface response in South China, Earth-Science Reviews, 243, 104496, https://doi.org/10.1016/j.earscirev.2023.104496, 2023.

Li, S. Z., Suo, Y. H., Li, X. Y., Zho, J., Santosh, M., Wang, P. C., Wang, G. Z., Guo, L. L., Yu, S. Y., Lan, H. Y., Dai, L. M., Zhou, Z. Z., Cao, X. Z., Zhu, J. J., Liu, B., Jiang, S. H., Wang, G., and Zhang, G. W.: Mesozoic tectono-magmatic response in the East Asian ocean-continent connection zone to subduction of the Paleo-Pacific Plate, Earth-Science Reviews, 192, 91-137, https://doi.org/10.1016/j.earscirev.2019.03.003, 2019.

Li, X. H.: Cretaceous magmatism and lithospheric extension in Southeast China, Journal of Asian Earth Sciences, 18, 293-305, https://doi.org/10.1016/S1367-9120(99)00060-7, 2000.

Li, Y. J., Lin, L., and Zhao, J. B.: A new model of the formation of the meso-cenozoic block basins in east China, Oil Gas Geology, 9, 334-345, https://doi.org/10.11743/ogg19880403, 1988.

Li, Z. X. and Li, X. H.: Formation of the 1300-km-wide intracontinental orogen and postorogenic magmatic province in Mesozoic South China: A flat-slab subduction model, Geology, 35, 179-182, https://doi.org/10.1130/g23193a.1, 2007.

Lin, A. T., Watts, A. B., and Hesselbo, S. P.: Cenozoic stratigraphy and subsidence history of the South China Sea margin in the Taiwan region, Basin Research, 15, 453-478, https://doi.org/10.1046/j.1365-2117.2003.00215.x, 2003.

Liu, Y. X.: The active fractures in South China Coast, Marine Geology & Quaternary Geology, 5, 11-21, https://doi.org/10.16562/j.cnki.0256-1492.1985.03.002, 1985.

Melgar, D., Taymaz, T., Ganas, A., Crowell, B., Öcalan, T., Kahraman, M., Tsironi, V., Yolsal-Çevikbilen, S., Valkaniotis, S., Irmak, T. S., Eken, T., Erman, C., Özkan, B., Dogan, A. H., and Altuntaş, C.: Sub- and super-shear ruptures during the 2023 Mw 7.8 and Mw 7.6 earthquake doublet in SE Türkiye, Seismica, 2, https://doi.org/10.26443/seismica.v2i3.387, 2023.

Morley, C. K.: Major unconformities/termination of extension events and associated surfaces in the South China Seas: Review and implications for tectonic development, Journal of Asian Earth Sciences, 120, 62-86, https://doi.org/10.1016/j.jseaes.2016.01.013, 2016.

https://doi.org/10.5194/nhess-2024-170
Preprint. Discussion started: 5 March 2025

Muldashev, I. A., Pérez-Gussinyé, M., and Sobolev, S. V.: Modeling of Continental Normal Fault Earthquakes, Geochemistry Geophysics Geosystems, 23, e2022GC010615, https://doi.org/10.1029/2022gc010615, 2022.

Muraoka, H. and Kamata, H.: Displacement distribution along minor fault traces, Journal of Structural Geology, 5, 483-495, https://doi.org/10.1016/0191-8141(83)90054-8, 1983.

Okada, Y.: Surface deformation due to shear and tensile faults in a half-space, Bulletin of the Seismological Society of America, 75, 1135-1154, https://doi.org/10.1785/BSSA0750041135, 1985.

Pedoja, K., Shen, J. W., Kershaw, S., and Tang, C.: Coastal Quaternary morphologies on the northern coast of the South China Sea, China, and their implications for current tectonic models: A review and preliminary study, Marine Geology, 255, 103-117, https://doi.org/10.1016/j.margeo.2008.02.002, 2008.

Pedoja, K., Regard, V., Husson, L., Martinod, J., Guillaume, B., Fucks, E., Iglesias, M., and Weill, P.: Uplift of quaternary shorelines in eastern Patagonia: Darwin revisited, Geomorphology, 127, 121-142, https://doi.org/10.1016/j.geomorph.2010.08.003, 2011.

Petricca, P., Bignami, C., and Doglioni, C.: The epicentral fingerprint of earthquakes marks the coseismically activated crustal volume, Earth-Science Reviews, 218, 103667, https://doi.org/10.1016/j.earscirev.2021.103667, 2021.

Petricca, P., Barba, S., Carminati, E., Doglioni, C., and Riguzzi, F.: Graviquakes in Italy, Tectonophysics, 656, 202-214, https://doi.org/10.1016/j.tecto.2015.07.001, 2015.

Pratt, T. L., Shaw, J. H., Dolan, J. F., Christofferson, S. A., and Plesch, A.: Shallow seismic imaging of folds above the Puente Hills blind-thrust fault, Los Angeles, California, Geophysical Research Letters, 29, 14–18, https://doi.org/10.1029/2001GL014313, 2002.

Qiu, Y., Huang, W., Du, W., and Han, B.: Analysis on the Formation of the Thin Continental Crust in the South China Sea, Earth Science, 46, 899-915, https://doi.org/10.3799/dqkx. 2020.393, 2021.

Savage, J. C. and Walsh, J. B.: Gravitational energy and faulting, Bulletin of the Seismological Society of America, 68, 1613-1622, 1978.

Shaw, J. H., Shearer, and M, P.: An elusive blind-thrust fault beneath metropolitan Los Angeles, Science, 283, 1516-1518, https://doi.org/10.1126/science.283.5407.1516, 1999.

Suppe, S. C.: Three-dimensional imaging of active structures using earthquake aftershocks: the Northridge thrust, California, Journal of Structural Geology, 24, 887–904, https://doi.org/10.1016/S0191-8141(01)00110-9, 2002.

Wang, S., Zhang, D., Wu, G. G., Vatuva, A., Di, Y. J., Yan, P. C., Feng, H. B., and Ma, S.: Late Paleozoic to Mesozoic extension in southwestern Fujian Province, South China: Geochemical, geochronological and Hf isotopic constraints from basic-intermediate dykes, Geoscience Frontiers, 8, 529-540, https://doi.org/10.1016/j.gsf.2016.05.005, 2017.

Wang, S. W., Zhan, W. H., Zhang, F., and Zhu, J. J.: The coulomb stress change associated with the Taiwan Strait MS7. 3 earthquake on Sep. 16, 1994 and the risk prediction of its surrounding faults, Earthquake Research in China, 27, 419-430, 2011.

Wang, X., Wei, S., Morales-Yáñez, C., Duputel, Z., Chen, L., Hao, T. Y., and Zhao, L.: Plate interface geometry complexity and persistent heterogenous coupling revealed by a high-resolution earthquake focal mechanism catalog in Mentawai, Sumatra, Earth and Planetary Science Letters, 637, https://doi.org/10.1016/j.epsl.2024.118726, 2024.

Wang, Y.: Heat flow pattern and lateral variations of lithosphere strength in China mainland: constraints on active deformation, Physics of the Earth and Planetary Interiors, 126, 121-146, https://doi.org/10.1016/s0031-9201(01)00251-5, 2001.

https://doi.org/10.5194/nhess-2024-170
Preprint. Discussion started: 5 March 2025

Withjack, M. O., Olson, J., and Peterson, E.: Experimental-models of extensional forced folds, Aapg Bulletin-American Association of Petroleum Geologists, 74, 1038-1054, https://doi.org/10.1016/0148-9062(91)92173-V, 1990.

Xia, S. H., Zhou, P. X., Zhao, D. P., and Cao, J. H.: Seismogenic structure in the source zone of the 1918 M7.5 NanAo earthquake in the northern South China Sea, Physics of The Earth Planetary Interiors, 302, 106472, https://doi.org/10.1016/j.pepi.2020.106472, 2020.

Xu, H. L., Qiu, X. L., Zhao, M. H., Sun, J. L., and Zhu, J. J.: Characteristics of the crustal structure and hypocentral tectonics in the epicentral area of Nan'ao earthquake (M7.5), the northeastern South China Sea, Chinese Science Bulletin, 51, 95-106, https://doi.org/10.1007/s11434-006-9095-x, 2006.

Xu, Y., Lü, Q. T., Shi, D. N., Zhang, Y. Q., Yan, J. Y., and Xu, Z. W.: Upper mantle velocity structure beneath the eastern South China Block and implications for late Mesozoic magmatism, Journal of Asian Earth Sciences, 224, https://doi.org/10.1016/j.jseaes.2021.105013, 2022.

Yang, S. X., Qiu, Y., Zhu, B. D., Chen, J., Guan, Y. X., Peng, X. C., et al: Atlas of Geology and Geophysics of the South China Sea, China Navigation Publications, 654-666, https://doi.org/10.3799/dqkx.2012.075, 2015.

Yi, H., Zhan, W. H., Min, W., Wu, X. C., Li, J., Feng, Y. C., and Ren, Z. K.: A comparative study of source effect based on mini-multichannel seismic profile in marine active fault detection, Seismology and Geology, 44, 333-348, https://doi.org/10.3969/j.issn.0253-4967.2022.02.004, 2022.

Zehnder, A. T. and Allmendinger, R. W.: Velocity field for the trishear model, Journal of Structural Geology, 22, 1009-1014, https://doi.org/10.1016/s0191-8141(00)00037-7, 2000.

Zhan, W. H., Zhang, Q. M., Sun, Z. X., Tang, C., and Qiu, X. L.: Geologic and geomorphologic characteristics and geological hazards of Nanpeng Archipelago and adjacent waters, northeastern South China sea, Journal of tropical oceanography, 21, 11-17, 2002.

Zhang, L., Liu, Y. J., Li, D., Yu, H. Y., and He, C. R.: Geometric Control on Seismic Rupture and Earthquake Sequence Along the Yingxiu-Beichuan Fault With Implications for the 2008 Wenchuan Earthquake, Journal of Geophysical Research-Solid Earth, 127, https://doi.org/10.1029/2022jb024113, 2022.

Zhang, Y., Yao, H., Yang, H.-Y., Cai, H.-T., Fang, H., Xu, J., Jin, X., Kuo-Chen, H., Liang, W.-T., and Chen, K.-X.: 3-D Crustal Shear-Wave Velocity Structure of the Taiwan Strait and Fujian, SE China, Revealed by Ambient Noise Tomography, Journal of Geophysical Research-Solid Earth, 123, 8016-8031, https://doi.org/10.1029/2018jb015938, 2018.

Zhang, Y. J., Tang, X. W., Liu, D. C., Taymaz, T., Eken, T., Guo, R. M., Zheng, Y., Wang, J. Q., and Sun, H. P.: Geometric controls on cascading rupture of the 2023 Kahramanmaras earthquake doublet, Nature Geoscience, 16, 1054-+, https://doi.org/10.1038/s41561-023-01283-3, 2023.

Zhang, Y. X., Ye, X. W., Wan, K. Y., Lv, Z. Y., Wen, G. G., and Xu, S. S.: Fault structure, seismicity, and magmatism of the Littoral Fault zone, northern South China sea: Insights from high-resolution seismic reflection data, Marine and Petroleum Geology, 160, 106605, https://doi.org/10.1016/j.marpetgeo.2023.106605, 2024.

Zhao, M. H., Qiu, X. L., Ye, C. M., Xia, K. Y., Huang, C. L., Xie, J. B., and Wang, P.: Analysis on deep crustal structure along the onshore-offshore seismic profile across the Binhai (littoral) fault zone in northeastern South China Sea, Chinese Journal of Geophysics-Chinese Edition, 47, 845-852, https://doi.org/10.3321/j.issn:0001-5733.2004.05.016, 2004.

https://doi.org/10.5194/nhess-2024-170
Preprint. Discussion started: 5 March 2025

Natural Hazards and Earth System Sciences
Discussions

Zhao, X. and Yao, Z. X.: The kinematic characteristics of the 2016 Mw7.8 offshore Sumatra, Indonesia earthquake, Chinese Journal of Geophysics-Chinese Edition, 61, 880-888, https://doi.org/10.6038/cjg2018K0624, 2018.

Zhou, D., Yu, H. S., Xu, H. H., Shi, X. B., and Chou, Y. W.: Modeling of thermo-rheological structure of lithosphere under the foreland basin and mountain belt of Taiwan Tectonophysics, 379, 259-259, https://doi.org/10.1016/j.tecto.2003.11.003, 2004.